Biophysical Journal, Volume 96

Supporting Material

Sequence and crowding effects in the aggregation of a ten residue fragment derived from islet amyloid polypeptide

Eva Rivera, John Straub, and D. Thirumalai

Monomer Analysis: In the comparison between the monomer structures sampled in our simulation and Eisenberg's crystal structure, we first examined the kink angle (θ) in the monomers. We define θ as the angle formed by the Cα's of N^{21}, G^{24}, and L^{27}. In the crystal structure of hIAPP (21-27) $\theta \approx 109°$. We computed θ for each monomer structure in the 36 mM and 28 mM trajectories (~ 20000 structures in total for each simulation). A histogram of the angles sampled was generated using a bin size of 1° and the probability of each angle was then determined. The resultant distribution is shown in Fig. 7a for the 28 mM system.

We further examined the propensity for each residue to be in a β-strand conformation and compared these results to the conformation in the crystal structure. A residue is considered to be β if its φ and ψ dihedral angles fall within the polygon defined by (-180, 180), (-180, 126), (-162, 126), (-162, 108), (-144, 108), (-144, 90), (-50, 90), (-50, 180) in φ□ψ coordinate space [26] . For each structure, we determined whether a given residue was β and determined the probability for each residue to be β over the 36 mM and 28 mM trajectories. The histogram for the 28 mM system is shown in Figure 6b. In the Eisenberg crystal structure N^{21}, N^{22}, and I^{26} adopt a β-conformation while F^{23}, G^{24}, and A^{25} do not. Our results for both systems (Fig. 1 in the main text and Fig. 7) are in accordance with the conformations adopted by the monomer in the crystal structure.

We also computed the RMSD of hIAPP residues 21-27 with respect to the crystal structure [16] for the monomers in our simulations. The RMSD for each structure was calculated using the backbone N, α-carbon, and C atoms. A histogram of the RMSDs was generated using a 0.5 Å bin size. The results are shown in Figure 7c. Again, we observe that a significant portion of the structures sampled in both simulations have a relatively low RMSD compared to the crystal structure (from 1 Å – 1.5 Å). The detailed structural comparison between simulation and experiment validates the computational approach.

Table 1

	sequence	number of peptides	conc. (mM)	unit cell type	unit cell size (nm^3)
System I	hIAPP	2	36.4	ortho. box	91
System II	rIAPP	2	36.8	ortho. box	91
System III	hIAPP	2	28.0	trunc. octa.	121
System IV	rIAPP	2	27.9	trunc. octa.	121

Figure 7: (top left) Probability distribution of θ values for the two monomers of the 28 mM simulation. (top right) Probability of finding each residue of the hIAPP sequence in a β-strand configuration for the 28 mM simulation. The results are averaged over both monomers. (bottom left) Probability distribution of backbone RMSD's versus the crystal structure for the 36 mM and 28 mM simulations. The results are averaged over both monomers.

Figure 8: The initial β-sheet structures used in the umbrella simulations for hIAPP (top) and rIAPP (bottom).

Figure 9: The initial dimer structures used in the long dynamics for hIAPP (top) and rIAPP (bottom).

Figure 10: Projection of the hIAPP trajectories for C_p = 36 mM (top) and C_p = 28 mM (bottom) onto the first and second principal component axes.

Figure 11: (left) β-bridge initially formed in the rIAPP C_p = 28 mM simulation, centered on leucine 28 of both monomers (pink). Proline 29 (blue) and the two valines (brown) form a hydrophobic cluster that stabilizes the bridge. (right) Reorganized β-bridge structure, centered on the leucine 28 of monomer A (pink) and valine 27 of monomer B (brown). The rearrangement facilitates better contact between the leucine side-chain and the proline 28 ring (blue).

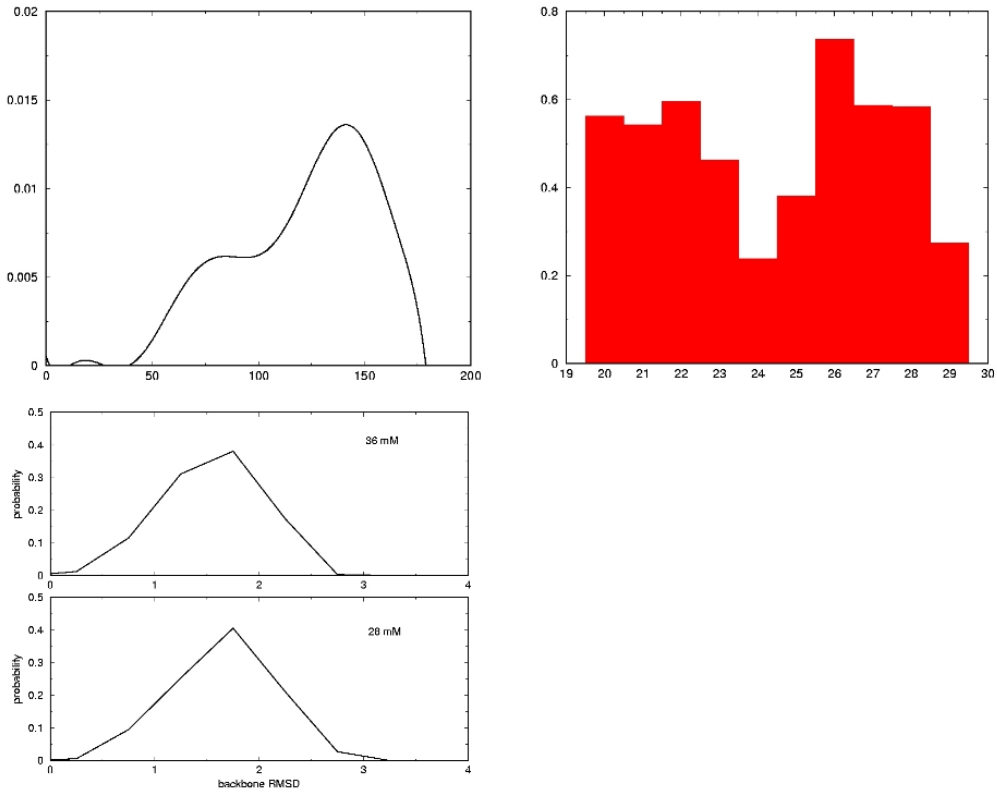
0.02
0.015
0.01
0.005
0
0
50
100
150
200
0.8
0.6
0.4
0.2
0
19
20
21
22
23
24
25
26
27
28
29
30
0.5
0.4
0.3
0.2
0.1
0
probability
36 mM
0
1
2
3
4
0.5
0.4
0.3
0.2
0.1
0
probability
28 mM
0
1
2
3
4
backbone RMSD

Figure 7

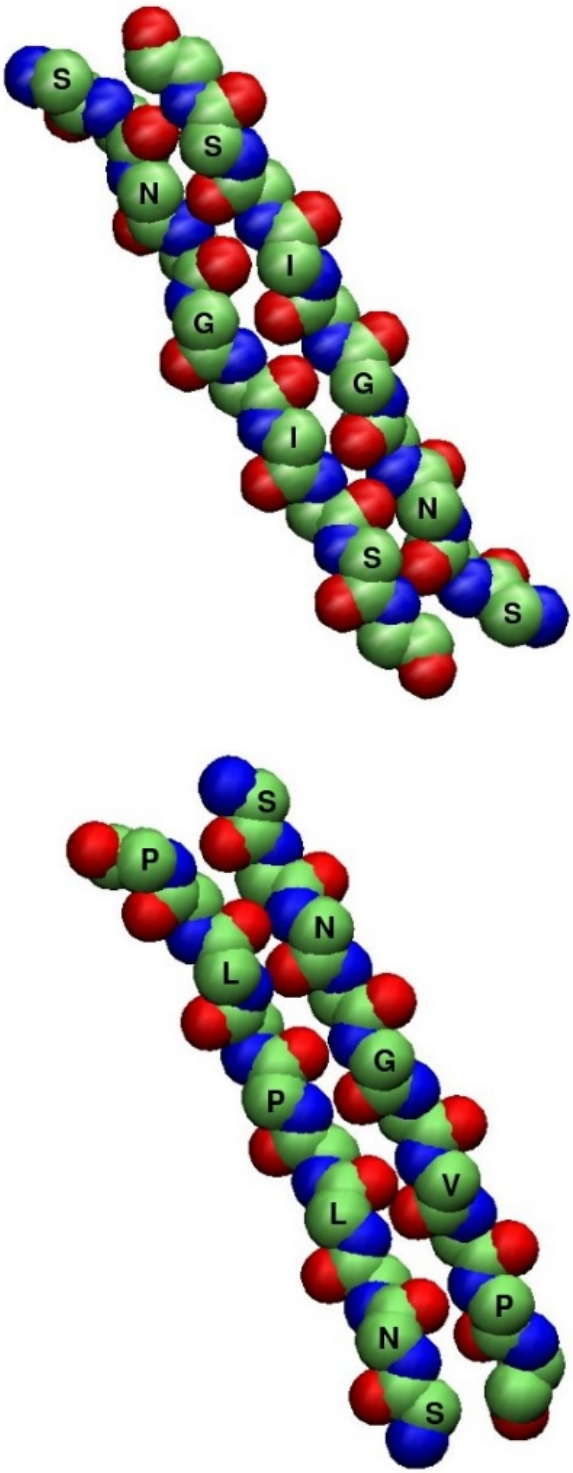

Figure 8

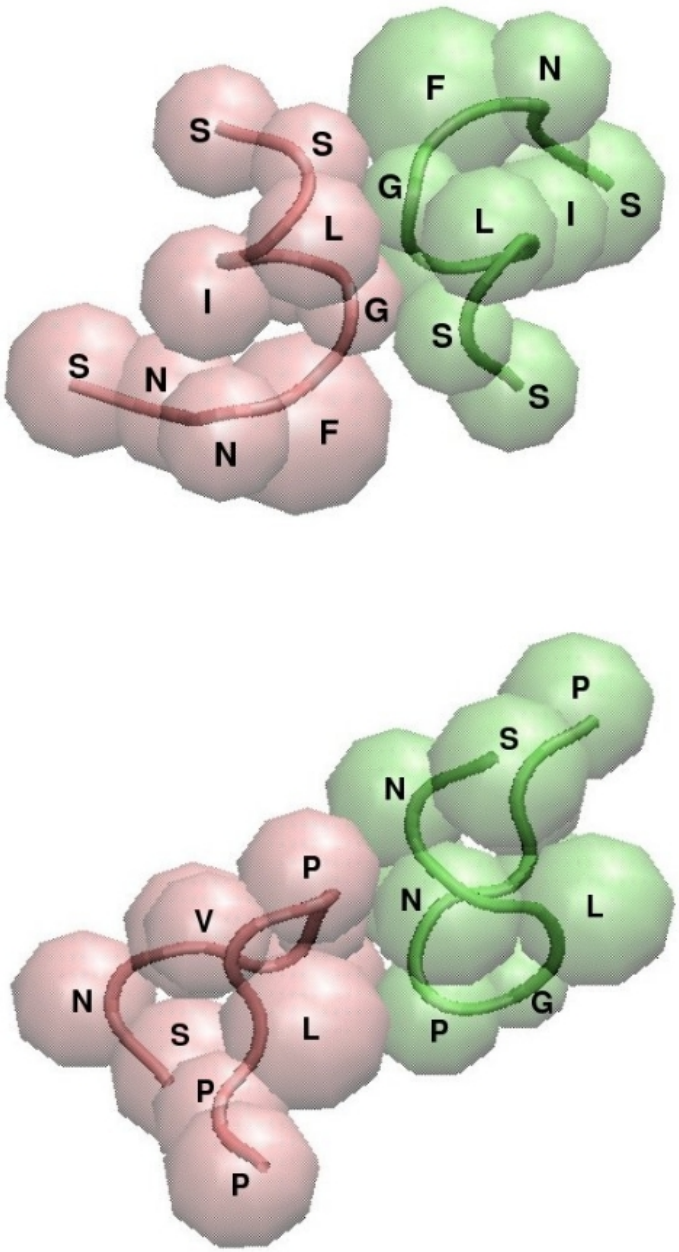

Figure 9

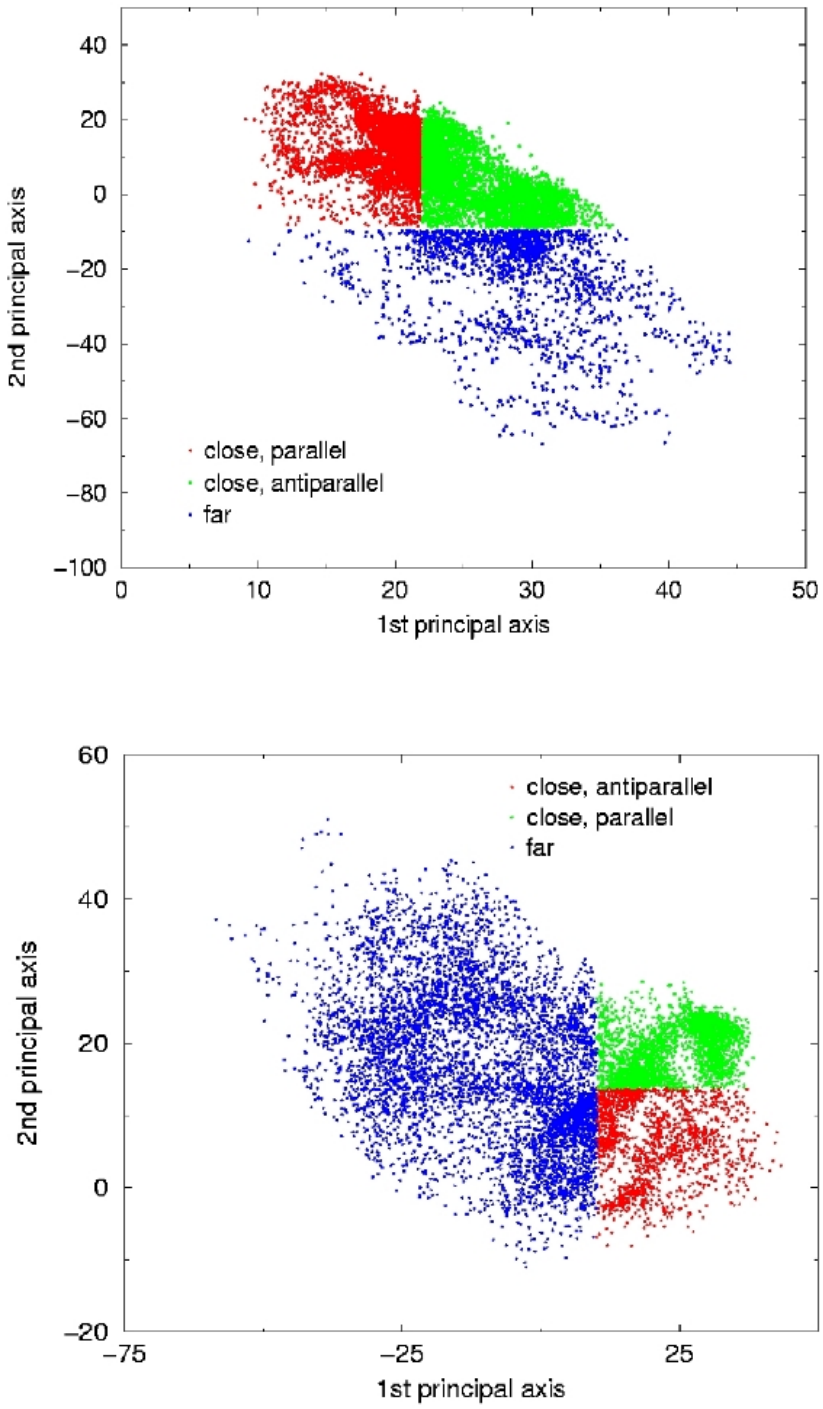
40
20
0
−20
−40
−60
−80
−100
0
10
20
30
40
50
2nd principal axis
1st principal axis
close, parallel
close, antiparallel
far
60
40
20
0
−20
−75
−25
25
2nd principal axis
1st principal axis
close, antiparallel
close, parallel
far

Figure 10

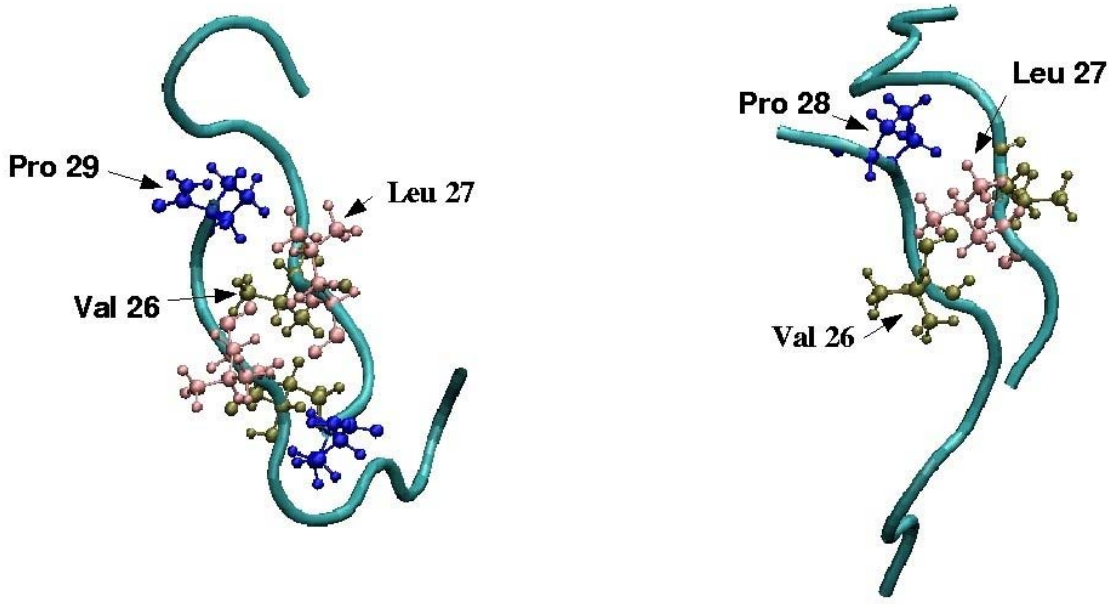

Figure 11